

1 **Temporal variability of tropospheric ozone and ozone**
2 **profiles in Korean Peninsula during the East Asian**
3 **summer monsoon: Insights from multiple**
4 **measurements and reanalysis datasets**

5
6 Juseon Bak^{1,*}, juseonbak@pusan.ac.kr

7 Eun-Ji Song^{1,a}, ejsong0510@gmail.com

8 Hyo-Jung Lee¹, hyojung@pusan.ac.kr

9 Xiong Liu², xliu@cfa.harvard.edu

10 Ja-Ho Koo³, zach45@yonsei.ac.kr

11 Joowan Kim⁴, joowan@kongju.ac.kr

12 Wonbae Jeon^{1,5}, wbyeon@pusan.ac.kr

13 Jae-Hwan Kim⁵, jaekim@pusan.ac.kr

14 Cheol-Hee Kim^{1,5,*}, chkim2@pusan.ac.kr

15
16 ¹*Institute of Environmental Studies, Pusan National University, Busan, South Korea*

17 ²*Smithsonian Astrophysical Observatory (SAO), Center for Astrophysics | Harvard & Smithsonian*

18 ³*Department of Atmospheric Sciences, Yonsei University, Seoul, Republic of Korea*

19 ⁴*Department of Atmospheric Sciences, Kongju National University, Kongju, South Korea*

20 ⁵*Department of Atmospheric Sciences, Pusan National University, Busan, South Korea*

21 ^a*Currently at [Supercomputer Center](#), Pukyong National University, Busan, South Korea*

22
23 *Corresponding Author**
24
25
26
27
28

29

Abstract

30 We investigate the temporal variations of the ground-level ozone and balloon-based ozone profiles at
31 Pohang (36.02°N, 129.23°E) in Korean Peninsula. Satellite measurements and chemical reanalysis products
32 are also intercompared to address their capability of providing a consistent information on the temporal and
33 vertical variability of atmospheric ozone. Sub-seasonal variations of the summertime lower tropospheric
34 ozone exhibit a bimodal pattern related to atmospheric weather patterns modulated by the East Asian
35 monsoon circulation. The peak ozone abundances occur during the pre-summer monsoon with enhanced
36 ozone formation due to favorable meteorological conditions (dry and sunny). Ozone concentrations reach
37 its minimum during the summer monsoon and then remerges in autumn before the winter monsoon arrives.
38 Profile measurements indicates that ground-level ozone is vertically mixed up 400 hPa in summer while
39 the impact of the summer monsoon on ozone dilution is found up to 600 hPa. Compared to satellite
40 measurements, reanalysis products largely overestimate ozone abundances in both troposphere and
41 stratosphere and give inconsistent features of temporal variations. Nadir-viewing measurements from the
42 Ozone Monitoring Instrument (OMI) slightly underestimate the boundary layer ozone, but well represent
43 the bimodal peaks of ozone in the lower troposphere and the interannual changes of the lower tropospheric
44 ozone in August, with higher ozone concentrations during the strong El Niño events and the low ozone
45 concentrations in during the 2020 La Niña event.

46

1. Introduction

48 ~~Ground level ozone~~ Ozone in the lower troposphere should be reduced due to its adverse effect as a
49 key air pollutant and greenhouse gas ~~in the troposphere~~, whereas stratospheric ozone should be protected
50 for life on the Earth due to its essential role in shielding harmful ultraviolet (UV) rays from the sun. Ozone
51 ~~is not directly emitted to the atmosphere, but formed through the photolysis of oxygen molecules (O₂) by~~
52 ~~strong UV strikes in the stratosphere as well as the photochemical process in which the photolysis of~~
53 ~~nitrogen dioxide (NO₂) by the lights below 420 nm yields ozone in the troposphere.~~

54 ~~This photochemical production has been strongly affected by the~~ The human activities damaging the
55 protective layer of the stratosphere with ~~the emissions~~ of ozone-depleting substances (e.g., ~~CFCs, Halon,~~
56 ~~HCFCs~~ halogen source gases) as well as ~~boosting the ground level ozone pollution~~ cause emissions of
57 tropospheric ~~the emission of~~ ozone precursors (~~CO, VOCs~~ nitrogen oxides, volatile organic compounds,
58 NO_x), which chemically react in the presence of sunlight producing tropospheric ozone. ~~— The~~

59 ~~photochemical~~ ~~In addition, the~~ formation and fate of ~~atmospheric~~ ozone ~~in the troposphere~~ is complicatedly
60 interacted with meteorology and climate variability (Jacob and Winner, 2009; Lu et al., 2019; Zhang and
61 Wang, 2016), making it difficult to evaluate impacts of the emission control measures on surface ozone
62 levels (Dufour et al., 2021). As well, the tropospheric ozone is strongly influenced by either downward
63 transport of stratospheric air masses or the horizontal transport of polluted air-masses (Langford et al., 2015;
64 Walker et al., 2010).

65 A monsoon is a major atmospheric circulation system affecting air mass transport, convection, and
66 precipitation in the middle and high latitudes. Lower tropospheric ozone and its precursors can be
67 significantly modulated by monsoonal changes on the physical and chemical processes to production, and
68 deposition and redistribution. The regional seasonality of ozone as well as the latitudinal differences in
69 ozone seasonality were attributed to the Asian monsoon-driven atmospheric circulation (~~Tanimoto et al.,~~
70 ~~2005~~; Worden et al., 2009). In particular, impacts of the East Asian summer monsoon (EASM) on
71 spatiotemporal variations of surface-layer ozone concentrations over China have been comprehensively
72 addressed (Gao et al., 2021; He et al., 2008; Li et al., 2018; McPeters et al., 2007; Shen et al., 2022; Yang
73 et al., 2014; Yin et al., 2019; Zhao et al., 2010). For example, Yin et al. (2019) characterized the
74 geographical distribution of ozone in China, with a bimodal structure of ozone with a summer trough in the
75 southern China whereas a unimodal cycle in the northern China. Shen et al., (2022) specified the source-
76 receptor relationships of ozone pollution over the central and eastern China, mainly modulated by the
77 monsoon circulation.

78 In view of the rainfall characteristics during EASM and its impact on tropospheric ozone over East Asia,
79 Korean Peninsula is one of the best regions worldwide. Korean Peninsula is located in the easternmost part
80 of the Asian continent adjacent to the West Pacific where more than a half of the total rainfall amount
81 is typically concentrated during a short rainy season called Jangma in summer, largely controlled by
82 the EASM (Choi et al., 2020; Ha et al., 2012). Therefore, understanding the EASM-induced changes in
83 chemical composition over the Korean peninsula is of importance, which has rarely been done in literature,
84 especially for ozone.

85 ~~The interannual and regional variabilities of monsoon rainfall patterns over Korean Peninsula have been~~
86 ~~continuously and extensively established (Choi et al., 2020; Ha et al., 2012), but rarely connected to impacts~~
87 ~~on the chemical composition.~~

88 The main objective of this paper is to characterize the temporal variability of tropospheric ozone and

- 서식 있음: 글꼴: Times New Roman
- 서식 있음: 글꼴: Times New Roman
- 서식 있음: 글꼴: Times New Roman
- 서식 있음: 글꼴: Times New Roman
- 서식 있음: 글꼴: Times New Roman
- 서식 있음: 글꼴: Times New Roman
- 서식 있음: 글꼴: Times New Roman
- 서식 있음: 글꼴: Times New Roman
- 서식 있음: 글꼴: Times New Roman
- 서식 있음: 글꼴: (한글) + 본문 한글(맑은 고딕)

89 ozone profiles, by linking with the meteorological variability largely controlled by the EASM. Ground-
90 based and balloon-based observations are collected from the Pohang station (36.02°N, 129.23°E) as a
91 reference dataset. The ground measurements are used to interpret the sub-seasonal variability of surface
92 ozone, while the vertical seasonality of ozone is investigated from ozonesondes. This paper is a preliminary
93 activity of the Asian Summer Monsoon Chemical and Climate Impact Project (ACCLIP) campaign
94 (<https://www2.acom.ucar.edu/acclip>) to investigate the impact of the Asian Summer Monsoon on regional
95 and global chemistry. The ACCLIP campaign will operate two aircrafts during the period July to August
96 in 2022 to measure atmospheric compounds through entire troposphere to lower troposphere over East Asia
97 and the West Pacific. The second objective of this paper is to evaluate whether the chemical reanalysis data
98 and remote-sensing data could represent a consistent picture of the summer monsoon impact on ozone
99 profile distribution. This evaluation will give an insight on the data selection used to fill in
100 the spatiotemporal gaps of the ACCLIP measurements.

101

102 2. Data descriptions

103 2.1 Ground measurements

104 Surface in-situ measurements of O₃ and NO₂ are collected from air quality monitoring networks of the
105 National Institute of Environmental Research (NIER) (AirKorea, <http://www.airkorea.or.kr>). This network
106 measures hourly air pollutants (O₃, NO₂, CO, SO₂) mixing ratios through the chemiluminescence
107 technology (Kley and Mcfarland, 1980). The KMA operates automatic synoptic observation system (ASOS)
108 at 102 weather stations. The ASOS measurements are provided in five types of time scales (minutely, hourly,
109 daily, monthly, yearly) via the KMA Weather Data Service (<https://data.kma.go.kr/>). We used daily
110 averages of air temperature, relative humidity, solar irradiance, total precipitation, wind speed, and wind
111 direction.

112

113 2.1.2 In-situ measurements Ozonesonde-measurements

114 Ozonesondes are balloon-borne instruments capable of measuring the vertical distribution
115 of atmospheric ozone from the surface to balloon burst, usually near 35 km. The electrochemical
116 concentration cell (ECC)-typed sensor is the most widely employed. ECC ozonesondes have an uncertainty
117 of 5 %–10 % and a precision of 3 %–5 % (Smit et al., 2007). In South Korea, only at the Pohang station

서식 있음: 들여쓰기: 첫 줄: 1 글자

서식 있음: 들여쓰기: 첫 줄: 1 글자

118 ECC sondes have been regularly launched every Wednesday in the afternoon (13:30-15:30 LT) since 1995.
119 Ozone measurements are reported in units of partial pressure (mPa) with vertical resolution of about
120 100 m by the Korea Meteorological Administration (KMA). Bak et al. (2019) demonstrated that Pohang
121 ozonesonde measurements are a stable set of reference profiles for validating satellite products, with the
122 comparable quality of ECC ozonesonde measurements in Japan and Hong Kong. To improve the data
123 quality data analysis, we screened out sounding measurements at with the balloon burst altitudes
124 higher lower than 200 hPa, and and abnormal observation concentrations of such as either tropospheric
125 ozone column values above 80 DU or stratospheric ozone column values below 100 DU as well as gaps
126 greater than 3 km.

127 ~~Surface in situ measurements of O₃ and NO₂ are collected from air quality monitoring networks of the~~
128 ~~National Institute of Environmental Research (NIER) (AirKorea, <http://www.airkorea.or.kr>). This network~~
129 ~~measures hourly air pollutants (O₃, NO₂, CO, SO₂) mixing ratios through the chemiluminescence~~
130 ~~technology (Kley and Mearland, 1980). The KMA operates automatic synoptic observation system (ASOS)~~
131 ~~at 102 weather stations. The ASOS measurements are provided in five types of time scales (minutely, hourly,~~
132 ~~daily, monthly, yearly) via the KMA Weather Data Service (<https://data.kma.go.kr/>). We used daily~~
133 ~~averages of air temperature, relative humidity, solar irradiance, total precipitation, wind speed, and wind~~
134 ~~direction.~~

135 **2.2.3 Satellite measurements**

136 Both OMI and MLS were launched on board of NASA's EOS-Aura spacecraft in July 2004 and
137 still functioning in measuring the Earth's atmospheric composition. The Aura satellite crosses the equator
138 at ~ 1:30 in the afternoon. OMI is a nadir-viewing imaging spectrometer capable of daily, global mapping
139 at relatively high spatial resolution of 13 km × 24-48 km (across × along track). MLS measures microwave
140 thermal emission from the limb of Earth's atmosphere. Compared to OMI, MLS makes measurements at a
141 good vertical resolution (~ 3 km) in the upper atmosphere, but at relatively coarse horizontal resolutions
142 (~165 km along the orbit track). The version 4.2 of the MLS standard ozone product is used in this study,
143 only for the recommended vertical range from 261 to 0.025 hPa (Schwartz et al., 2015). We used OMI
144 ozone profiles retrieved using the PROFOZ version 2 algorithm which is in preparation for reprocessing
145 OMI measurements to release a new version of the OMPROFOZ research product (Liu et al., 2010). This
146 retrieval algorithm consists of wavelength/radiometric calibrations and forward modeling simulations, with
147 an optimal estimation inversion where a priori knowledge is optimally combined with measurement

148 information to obtain a better estimate of the state (Rodgers, 2000). The measurement sensitivity inherently
149 decreases toward the surface, with the increasing dependence of retrievals on the a priori information (Bak
150 et al., 2013). OMI sensitivity is very low to surface ozone, with its maximum in the free troposphere (~500
151 hPa) (Shen et al., 2019).

152 **2.3.4 Reanalysis data**

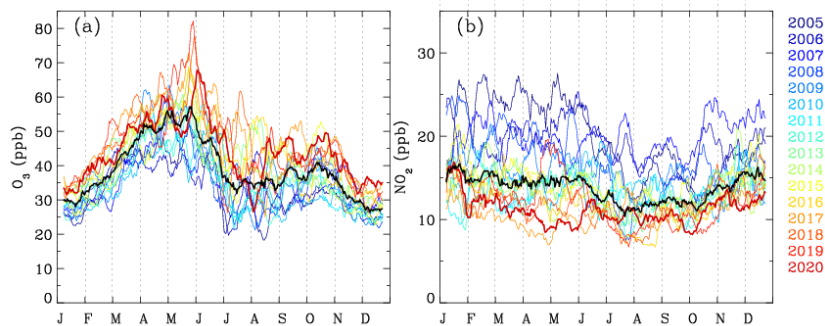
153 The Modern-Era Retrospective Analysis for Research and Applications, version 2 (MERRA-2), is
154 NASA's latest reanalysis, spanning the satellite observing era from 1980 to the present (Gelaro et al.,
155 2017). In addition to a standard meteorological analysis, a global O₃ field is driven by atmospheric
156 dynamics and constrained by satellite O₃ measurements using the GEOS-5 atmospheric model and the data
157 assimilation system. Beginning in October 2004, MERRA-2 assimilates total column ozone from OMI and
158 stratospheric ozone profiles above 215 hPa from MLS. Note that OMI total column ozone is assimilated to
159 account for the lower sensitivity of MLS measurements in the lower stratosphere, specifically in clouded
160 scenes.

161 The CAMS reanalysis is the latest global reanalysis data set of atmospheric composition produced by the
162 Copernicus Atmosphere Monitoring Service (CAMS), covering the period from 2003 to present (Inness et
163 al., 2019). Compared to MERRA-2, multiple satellite measurements were assimilated for the CAMS
164 reanalysis with ECMWF's Integrated Forecasting System. These included total ozone columns from
165 SCIAMARCY, OMI, and GOME/2 as well as ozone profiles from MIPAS and MLS after 2005.

166 Both reanalysis data have similar temporal and spatial resolutions. Merra-2 system produces 3-hourly
167 analyses at 72 sigma-pressure hybrid layers between the surface and 0.01 hPa, with a
168 horizontal resolution of $0.625^\circ \times 0.5^\circ$. The CAMS reanalysis data provide estimates every 3 hours with a
169 horizontal resolution of $0.75^\circ \times 0.75^\circ$. The vertical resolution of model consists of 60 hybrid sigma-pressure
170 (model) levels from surface to 0.1 hPa. In this study, we used CAMS global reanalysis (EAC4) monthly
171 averaged fields at 25 pressure levels (1000 hPa to 1 hPa) as well as MERRA-2 monthly mean data at 42
172 pressure levels (1000 hPa to 1 hPa). Both datasets provide ozone profiles in the unit of mixing ratio.

173 **3. Results and discussion**

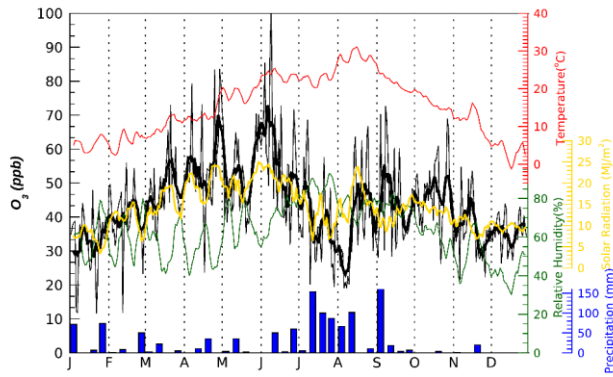
174 **3.1. Temporal variability of ground-level ozone**



175
 176 **Figure 1.** (a) Two-week moving averages of daytime ground-level ozone concentrations monitored at 6
 177 sites in Pohang, with (b) corresponding NO₂ concentrations. Different colorings represent each year from
 178 2005 to 2020, while the black line represents the mean ozone concentrations from all years.

179
 180 Figure 1 shows both interannual and seasonal changes of daily ground-level concentrations of O₃
 181 averaged at six AirKorea sites located within Pohang for 16 years (2005-2020) in comparison with its
 182 primary precursor NO₂. Pohang is a major industrial city on South Korea's east coast, with the largest
 183 population of North Gyeongsang Province. In this analysis, hourly measurements in afternoon (1-3 pm
 184 local time) are first averaged for a given calendar day and then smoothed by two-week moving average.
 185 The afternoon NO₂ do not change much seasonally. However, the seasonal cycle of ozone is bimodal with
 186 peaks in early-summer and fall. Ozone concentration rapidly increases from ~ 30 ppb in January to primary
 187 peak values of ~ 55 ppb on average during the period of late May to early June. The second peak of ozone
 188 occurs in fall, which is much lower than the major peak.

189
 190 In wintertime, the annual minimum of ozone concentrations gradually increases by ~ 10 ppb during
 191 last 15 years whereas the annual maximum of summertime ozone rapidly increases from ~ 40 ppb to 80
 192 ppb, in spite of the reduction of NO₂ amount by ~ 15 ppb or larger. [Both depth and width of the summer](#)
 193 [trough are highly variable, likely influenced by the strength and duration of the summer monsoon \(Yang et](#)
[al., 2014; Zhou et al., 2022\).](#)



194
 195 **Figure 2.** (Black) Daily ground-level ozone concentrations where weekly moving averages are applied
 196 (thick line) or not (thin line) at Pohang in 2020. The corresponding meteorological factors are overplotted;
 197 surface air temperature (red, °C), solar radiation (yellow, MJ/m²), and relative humidity (dark green, %).
 198 The bar graph shows the total precipitation (mm) for each week.

199 **Table 1.** Same as Figure2, but for correlation coefficients between ozone and meteorological variables, for
 200 pre-summer, summer, and post-summer periods, respectively.

	pre-summer (Jan-May)	Summer (Jun-Aug)	Post-summer (Sep-Dec)
Solar radiation	0.91	0.74	0.51
Air temperature	0.79	-0.15	0.69
Relative humidity	-0.27	-0.64	0.59

201
 202 In order to avoid smoothing out important features of intra-summer variations in ozone and their
 203 association with synoptic weather patterns, daily ozone and meteorological variables are zoomed in 2020
 204 as one-week moving average (Figure 2). The local maximum of ozone concentrations is generally tied to
 205 the local warm, dry air and intense solar radiation before the rainy season starts. This is indicating that both
 206 depth and width of the summer trough could be highly variable, likely influenced by the strength and
 207 duration of the summer monsoon (Yang et al., 2014; Zhou et al., 2022).

208 -The correlation between ozone concentrations and meteorological variables is quantitatively compared
 209 in Table 1, for summer and post/pre-summer periods, respectively. Solar insolation amounts are directly
 210 linked to ozone concentrations over all seasons (r=0.51-0.91). The significant relationship between ozone
 211 and air temperature is also identified before and after summer seasons. However, in summer, ozone

서식 있음: 들여쓰기: 첫 줄: 0.58 cm

서식 있음: 글꼴: Times New Roman

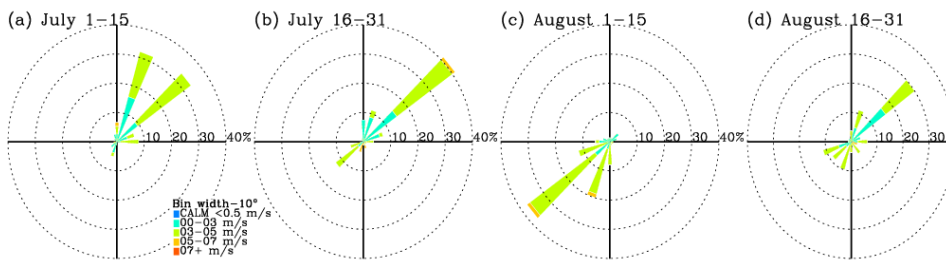
서식 있음: 글꼴: Times New Roman

서식 있음: 글꼴: Times New Roman

서식 있음: 글꼴: Times New Roman

서식 있음: 글꼴: Times New Roman

212 variations are rarely linked with temperature variations, due to the intense precipitation suppressing ozone
 213 formation. Consequently, the local minimum of ozone levels is tied to the local maximum of the relative
 214 humidity during the rainy season ($r=-0.64$). Note that the relative humidity is significantly influenced by
 215 air temperature, rather than amount of water vapor in the pre and post summer periods. Therefore, in the
 216 post summer the correlation of ozone with relative humidity ($r=0.59$) is likely to arise from the correlation
 217 of ozone with air temperature ($r=0.51$). The rapid drop of ~ 10 ppb in ozone from the end of July to early
 218 August is hardly explained with meteorological factors mentioned above; the weather becomes warmer
 219 with other meteorological variables (precipitation and solar radiation) being relatively invariant. However,
 220 the prevailing wind is characterized as southwesterlies in early August, exceptionally. Note that the
 221 northwesterly winds were dominant in July and in late August (see. Figure 3). This summer minimum could
 222 deepen with the inflow of the poor ozone air mass originated from the southern sea off the Korean peninsula
 223 into inland.



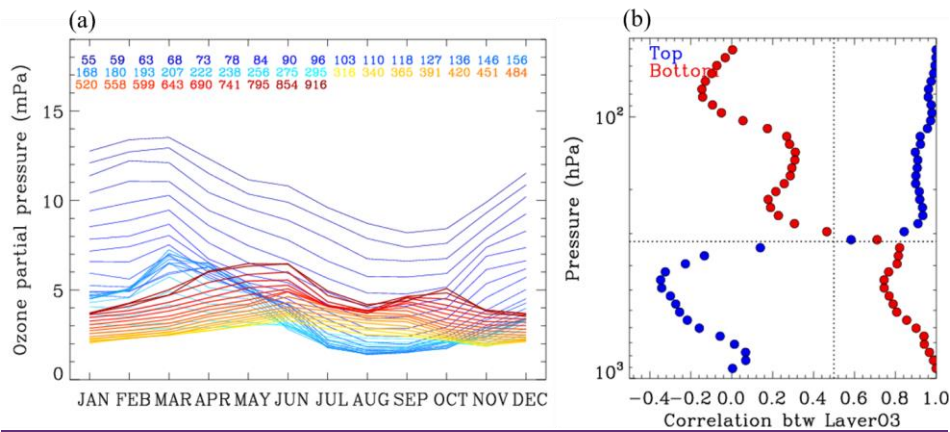
224
 225 **Figure 3.** Wind roses for individual months from June through September in 2020 at Pohang. Note that
 226 hourly observations in daytime are used to be consistent with data processing done in Figures 1 and 2.
 227

228 **3.12. Temporal variability of ozone profiles**

229 To understand the seasonality of ozone profiles, ozonesonde measurements collected at Pohang station
 230 are climatologically averaged for each month and each pressure bin (~ 0.5 km intervals). Ozonesondes
 231 soundings mainly measure ozone in the lower atmosphere below 10hPa while space-based limb soundings
 232 mainly measure ozone in the upper atmosphere above 215hPa. However, both sounding measurements
 233 provide the limited spatiotemporal information. OMI nadir measurements and reanalysis data provide the
 234 daily global maps of ozone profiles. but the reliability of those data products should be assured before using
 235 them to interpret ozone variability and its linkage to the monsoon circulation. As shown in Figure 4a, two

236 kinds of seasonal patterns are identified with a bimodal structure of layer ozone partial pressures in the
 237 lower troposphere (LT) whereas a unimodal cycle in the upper troposphere and lower stratosphere (UTLS).
 238 The LT ozone concentrations are peaked at June and October with a global minimum in winter as well as
 239 a local summer minimum in late July and early August, which is consistent with surface measurements.
 240 The concentrations of UTLS ozone are relatively higher in March due to the stratospheric intrusion, while
 241 the minimum concentrations appear broadly over the summer and early fall due to the rise of the tropopause,
 242 which is a common feature of ozone in the extratropical UTLS (Gettelman et al., 2011; Rao et al., 2003).
 243 In order to quantify the similarity of seasonal variations, the correlation coefficient is calculated for
 244 temporal ozone changes between each layer and the top/bottom layer. As shown in Fig. 4. b. the seasonality
 245 of ozone at 50 hPa is significantly correlated down to ~ 300 hPa, with the correlation coefficient of larger
 246 than 0.8. In addition, ozone in the boundary layer is significantly correlated with the lower tropospheric
 247 ozone up to 700 hPa ($r > 0.9$) as well as the upper tropospheric ozone up to ~ 300 hPa ($r = 0.7-0.8$). It illustrates
 248 that the 300 hPa could be regarded as a chemical barrier working as a boundary between troposphere and
 249 stratosphere at Pohang.

250



251

252 **Figure 4.** (a) Monthly variations of layer ozone partial pressures from ozonesonde soundings obtained from
 253 Pohang during the period of 2005 to 2020. The legend values indicate the midpoint pressure of the layer
 254 (hPa). (b) Correlation coefficients of monthly ozone variations between each layer and bottom layer (916
 255 hPa in red)/top layer (55 hPa in green).

256 In Figure 5, monthly averaged ozonesonde profiles are presented for 2020 and compared as a reference
 257 to assess satellite measurements and reanalysis products. This contour map of ozonesondes clearly

서식 있음: 글꼴: Times New Roman

서식 있음: 글꼴: Times New Roman

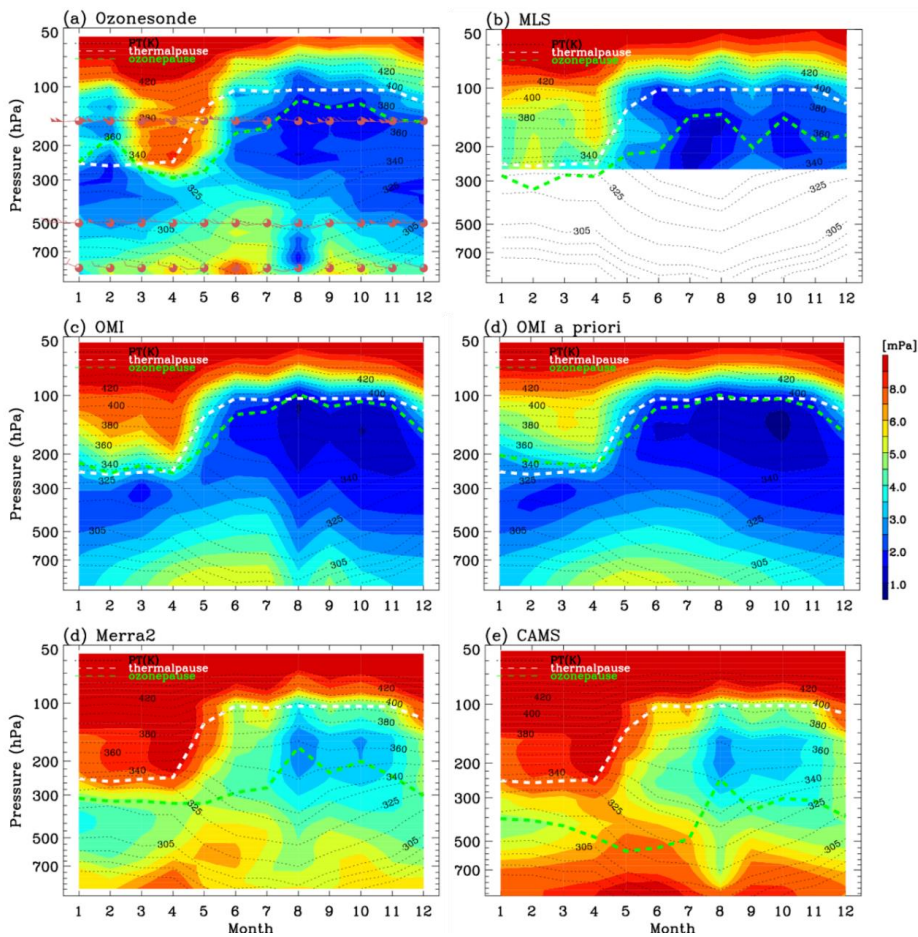
서식 있음: 글꼴: Times New Roman

서식 있음: 글꼴: Times New Roman

258 illustrates the intrusion depth of the stratospheric air masses down to ~ 300 hPa during spring months (Fig
259 5a). The mixing depth of ozone that forms near the ground level is also identified, which is bounded up to
260 ~400 hPa in the summer and ~600 hPa in other seasons. The minimum ozone concentration is typically
261 found just below the thermal tropopause. The August minimum of the lower tropospheric ozone is vertically
262 extended above ~600 hPa. This air mass is much cleaner compared to the winter ozone concentration over
263 the lower troposphere. The dominant factor suppressing the ozone formation is a long-lasting summer
264 precipitation from early July to mid-Aug in 2020 (Fig.2). Southerly wind that blows on the observation site
265 is relatively strong compared to June and July. Therefore, we could interpret that the inland polluted air
266 masses are likely to be diluted with the inflows of the maritime clean air masses as mentioned above. In the
267 lower troposphere, the minor peak of ozone concentrations is also identified in spring, which is not visible
268 in time-series plots of surface measurements (Fig. 2). The springtime peak is mainly originated by the fair
269 weather accelerating the formation of ground-level ozone with the wintertime accumulation of ozone and
270 its processors; it also could be partly attributed by the dynamical processes transporting the ozone-rich airs
271 from the UTLS and upwind areas. In Figures 5.b-f, OMI, MERRA-2, and CAMS ozone profiles are
272 qualitatively evaluated with respect to the capability of reproducing the seasonality of ozone profiles at
273 this location. The ozone minimum of summer monsoon season is detected from all ozone products, but
274 much broader than that in ozonesondes due to both the limited time resolution of ozonesonde measurements
275 and the limited spatial resolution of OMI and reanalysis products. OMI also show a very good agreement
276 with both ozonesonde in terms of reproducing the boundary layer ozone extending up to free troposphere
277 and low ozone concentration below the tropopause. In addition, the vertical gradient of ozone enhancement
278 above the tropopause is consistently reproduced from OMI, ozonesondes, and MLS. The spring ozone peak
279 near surface is not detectable from OMI measurements due to the limited sensitivity to relatively shallow
280 boundary layers compared to summer (Shen et al., 2019). In Figure 5.d, OMI a priori profile is also
281 presented to highlight that the summer minimum is derived from the independent information of OMI
282 measurements, rather than a priori information. It also illustrates that the summer minimum is a regional
283 feature of tropospheric ozone seasonality, not represented from the climatological data in which long-term
284 global measurements are composited as a function of month and latitude.

285 Both MERRA-2 and CAMS considerably overestimate ozone abundances in both troposphere and
286 stratosphere in spite of that MLS measurements are commonly employed for assimilating stratospheric
287 ozone profiles. In MERRA-2, the bimodal peaks (April and October) of the lower tropospheric ozone is
288 inconsistent with others (early summer, September). We also compare how each ozone product represents
289 the tropopause against thermally defined tropopause heights using the World Meteorological Organization

290 (WMO) definition (WMO, 1957). There is no universal method to define the ozonepause height, but
291 threshold values of 100 to 150 ppb in ozone mixing ratios were used to discriminate stratospheric to
292 tropospheric air masses (e.g., Hsu et al., 2005; Prather et al., 2011). In this paper, the 150 ppb value is
293 selected due to similarities of thermal tropopauses with ozone surfaces of 150 hPa from ozonesonde
294 measurements. As shown, the ozone surfaces at 150 ppb of reanalysis products are positioned in the free
295 troposphere due to the overestimation errors. Both ozonesonde and Aura measurements show somewhat
296 consistency between their ozone and thermal tropopause pressures. In particular, OMI shows the strong
297 consistency with the fact that retrievals near the tropopause are largely constrained with the a priori state
298 taken from the tropopause-based ozone profile climatology (Bak et al., 2013).



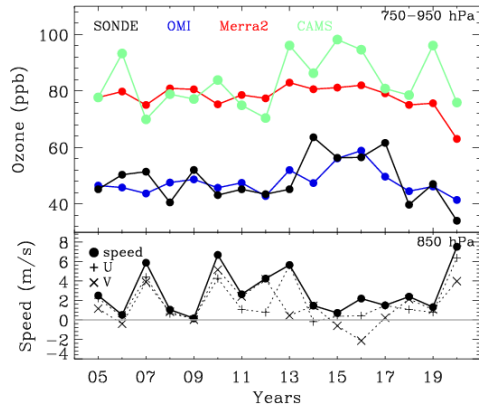
299
 300 **Figure 5.** Contour plots of monthly ozone profiles in 2020 from (a) ozonesonde, (b) MLS, (c) OMI, (d)
 301 OMI a priori, (e) MERRA-2, and (f) CAMS. The meteorological variables are superimposed for wind barbs
 302 (red symbols), potential temperatures (black contours), thermal tropopause heights (white lines) using
 303 monthly MERRA-2 meteorological data. The ozone value of 150 ppb is plotted with green lines for
 304 indicating the chemical transition between troposphere and stratosphere.

305 **3.23. Interannual variability of lower tropospheric ozone in summer**

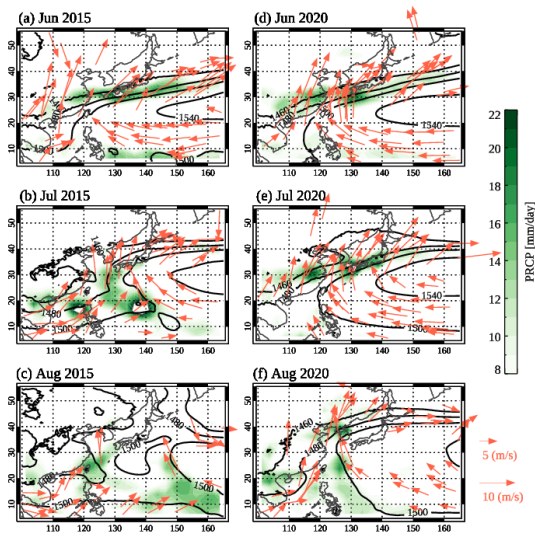
306 In this section, we focus on the ozone changes related to interannual meteorological variabilities, along
 307 with the evaluation of different ozone products. In Figure 6, the time-series of mean ozone mixing ratio in

308 the lower troposphere (750-950 hPa) in August are compared. The summer monsoon typically ends in the
309 late July and early August over Korean peninsula and hence the ozone abundance in August is sensitive to
310 the intensity and duration of the monsoon season. OMI and ozonesonde show a similar long-term change,
311 except for much more fluctuations in time-series of ozonesondes due to insufficient samplings (weekly
312 observations) used in monthly averages. A noticeable correlation ($r = \sim -0.52$) exists between wind speeds
313 and ozone mixing ratios (ozonesonde). Low wind speed could enhance the accumulation of ozone
314 precursors and the rate of ozone formation. Accordingly, both ozonesonde and OMI measurements detect
315 higher ozone abundances in August from 2014 to 2017 when the wind speeds are relatively lower. As
316 shown in Figure 7 (a-c), where the monthly meteorological fields at 850 hPa in 2015 are presented from
317 MERRA-2 product, the western North Pacific Subtropical High (WNPSH) was broken in August and hence
318 the weather was likely to be calm and dry over the Korean peninsula. Compared to past few years, the lower
319 amount of ozone is detected in 2020 from ozonesonde measurements. In August 2020, the lower
320 tropospheric southwesterly winds blow from the western North Pacific to Korean Peninsula across the edge
321 of WNPSH as well as the rain belt over Korean Peninsula (Fig. 7. d-f). Therefore, the weather was windy
322 and wet, suppressing ozone formation in August 2020.

323 MERRA-2 ozone shows no annual variation, before 2020 unlike other ozone measurements and product.
324 CAMS also shows the higher ozone concentrations correlated with wind speeds, but less consistent with
325 ozonesonde measurements compared to OMI. How the El Niño-Southern Oscillation (ENSO) cycle
326 interacts with the East Asian monsoon has been not established. According to the Oceanic Niño Index, the
327 2015-2016 El Niño event, the warm phase of the ENSO, was one of the strongest events ever recorded,
328 whereas the 2020-2021 La Niña event was also abnormally strong. There was a lot of unprecedented
329 weather events in south Korea during these super El Niño and La Niña periods, such as
330 unprecedented summer rainfalls in 2020 and unprecedented summer heatwaves in 2015-2016 (Yoon et al.,
331 2018). Therefore, we could relate the higher ozone amount in August 2015-2017 and the lower ozone
332 amount in August 2020 to a climatic forcing on the strength and position of WNPSH and hence the East
333 Asian summer climate.



334
 335 **Figure 6.** Annual variations of (top) the lower tropospheric ozone (750-950 hPa) in August from various
 336 ozone products, along with (bottom) the wind speeds at 850 hPa.



337
 338 **Figure 7.** The monthly meteorological fields at 850 hPa for (a-c) 2015 and (d-f) 2020, respectively. The wind vectors
 339 are drawn with the orange arrows. The geopotential heights are superimposed with black lines. The variations of
 340 precipitation are shown with green typed colors, respectively. Note that we use MERRA-2 meteorological variables
 341 except for the precipitation data taken from GPCP Version 2.3 Combined Precipitation Data Set (Adler et al., 2003).

342

343 **4 Summary and Conclusions**

344 In this paper, atmospheric ozone variabilities over Korean peninsula and their linkages to the East
345 Asian summer monsoon are vertically characterized using multiple ozone measurements made by surface
346 observation, balloon-borne ozonesonde, OMI, and MLS. MERRA-2 and CAMS are also integrated in this
347 analysis for the evaluation against ozonesonde. Surface in-situ measurements at six urban sites in Pohang
348 are averaged, while satellite and reanalysis datasets are spatially interpolated onto the Pohang ozonesonde
349 site. Surface measurements clearly show the impact of frequent weather changes (dry and wet) on ozone
350 concentrations in spring. The seasonality of ozone becomes very complicated in late spring to early fall,
351 depending on monsoon strengths and lengths. The peak concentration of ozone occurs in the pre-summer
352 monsoon season (~ 70 ppb) and in the post-summer monsoon season (~50 ppb). During the summer
353 monsoon, ozone concentrations decrease down to ~ 30 ppb, which is even lower than that in the winter
354 when the air temperature and solar insolation is lowest. The vertical structures of ozone concentrations
355 driven by the stratospheric dynamics and synoptic scale tropospheric weather disturbances are
356 characterized from ozonesonde soundings. The stratospheric intrusions actively occur from March to May
357 and modulate the upper tropospheric ozone, down to ~ 300 hPa. We identified ozone enhancements in the
358 boundary layer, extending up to 400 hPa in June. In August the monsoon-induced ozone dilution occurs in
359 the lower troposphere up to ~ 600 hPa. The ozone minimum also occurs just below the tropopause, which
360 is deepest from summer to early fall with the troposphere being extending upward to ~ 100 hPa. Both
361 satellite and reanalysis datasets show the capability of reproducing general features of ozone seasonality
362 such as bimodal peaks in ground-level ozone and spring maximum in the UTLS ozone. However, MERRA-
363 2 and CAMS products significantly overestimates ozone abundances in the UTLS and hence middle
364 tropospheric ozone concentrations exceed 150 ppb which is used as a chemical proxy to distinguish between
365 stratospheric air and tropospheric air. In general, OMI shows a good agreement with ozonesonde
366 measurements with respect to both seasonal tendency and quantitative terms, but slightly underestimates
367 ground-level ozone due to the limited vertical sensitivity. The lower tropospheric ozone in August shows
368 the monsoon-induced interannual variabilities with higher concentrations during the super El Niño and
369 lower concentration during the significant La Niña period, commonly from ozonesonde and OMI
370 measurements. However, MERRA-2 rarely shows long-term changes of August ozone in the lower
371 troposphere. On the other hand, CAMS is annually correlated with ozonesonde measurements, but with the
372 systematic positive biases of ~ 40 ppb. In conclusion, OMI could play a vital role in studying the impact of
373 summer monsoon-derived atmospheric circulation and weather on ozone seasonality. The analysis results
374 of this study could be a useful reference to the upcoming results from the ACCLIP campaign planned in

375 the summer of 2022 to gather comprehensive, integrated datasets of two airborne observations (Flight
376 Operations from S. Korea) and ground/balloon measurements, over the East Asia and Western Pacific.
377 ACCLIP measurements will provide useful ideas for better understanding the spatiotemporal variation of
378 ozone in the Korean peninsula in terms of continuous ozone increase near the surface (Yoo et al., 2015),
379 high ozone in the free troposphere (Crawford et al., 2021), and the relationship between the stratospheric
380 ozone intrusion and atmospheric circulation (Park et al., 2012).

381
382 **Author Contributions** J.B and C.K designed the research; E.S interpreted the reanalysis products
383 and H.L and W.J contributed on analyzing surface measurements. X.L contributed on OMI ozone profile
384 retrievals. C.K and J.A.K provided oversight and guidance for connecting the weather condition and air
385 pollutant concentrations. J.K and J.O.K contributed to the interpretation of the results. J.B lead the writing
386 of the manuscript; all co-authors contributed to discussion and edited the paper.

387 **Competing interests.** The authors have no competing interests

388 **Acknowledgement**

389 We thank the KMA, NIER, NASA, and Copernicus for providing their measurements and analysis data.
390 We hope that the 2022 ACCLIP campaign could successfully be processed in South Korea and the research
391 outcome would be fascinating. We would like to acknowledge the Basic Science Research Program
392 (2020R1A6A1A03044834 and 2021R1A2C1004984).

393 *Financial support.* This research has been supported by the Basic Science Research Program through the
394 National Research Foundation of Korea (NRF) funded by the Ministry of Education (grant
395 no. 2020R1A6A1A03044834 and 2021R1A2C1004984)

396 **Data Availability**

397 Ozonesonde: <https://data.kma.go.kr> (last access: 16 Jun 2022)
398 AirKorea: <http://www.airkorea.or.kr> (last access: 16 Jun 2022)
399 ASOS: <https://data.kma.go.kr> (last access: 16 Jun 2022)
400 OMI ozone profile retrievals: attainable upon request (juseonbak@pusan.ac.kr)
401 MLS Version 4.2 ozone profile: <https://earthdata.nasa.gov> (last access: 16 Jun 2022).
402 MERRA-2 reanalysis data: <https://gmao.gsfc.nasa.gov/reanalysis/MERRA-2/> (last access: 16 Jun 2022).
403 CAMS global reanalysis (EAC4): <https://ads.atmosphere.copernicus.eu/> (last access: 16 Jun 2022).
404 GPCP Version 2.3 Combined Precipitation Data Set: <https://psl.noaa.gov/> (last access:16 Jun 2022)
405

406 **References**

- 407
408 Bak, J., Liu, X., Wei, J. C., Pan, L. L., Chance, K. and Kim, J. H.: Improvement of omi ozone profile
409 retrievals in the upper troposphere and lower stratosphere by the use of a tropopause-based ozone
410 profile climatology, *Atmos. Meas. Tech.*, 6(9), 2239–2254, doi:10.5194/amt-6-2239-2013, 2013.
411 Bak, J., Baek, K. H., Kim, J. H., Liu, X., Kim, J. and Chance, K.: Cross-evaluation of GEMS tropospheric
412 ozone retrieval performance using OMI data and the use of an ozonesonde dataset over East Asia
413 for validation, *Atmos. Meas. Tech.*, 12(9), 5201–5215, doi:10.5194/amt-12-5201-2019, 2019.
414 Bethan, S., Vaughan, G. and Reid, S. J.: A comparison of ozone and thermal tropopause heights and the
415 impact of tropopause definition on quantifying the ozone content of the troposphere, *Q. J. R.*
416 *Meteorol. Soc.*, 122(532), 929–944, doi:https://doi.org/10.1002/qj.49712253207, 1996.
417 Choi, J.-W., Kim, H.-D. and Wang, B.: Interdecadal variation of Changma (Korean summer monsoon
418 rainy season) retreat date in Korea, *Int. J. Climatol.*, 40(3), 1348–1360,
419 doi:https://doi.org/10.1002/joc.6272, 2020.
420 Crawford, J. H., Ahn, J.-Y., Al-Saadi, J., Chang, L., Emmons, L. K., Kim, J., Lee, G., Park, J.-H., Park,
421 R. J., Woo, J. H., Song, C.-K., Hong, J.-H., Hong, Y.-D., Lefer, B. L., Lee, M., Lee, T., Kim, S.,
422 Min, K.-E., Yum, S. S., Shin, H. J., Kim, Y.-W., Choi, J.-S., Park, J.-S., Szykman, J. J., Long, R.
423 W., Jordan, C. E., Simpson, I. J., Fried, A., Dibb, J. E., Cho, S. and Kim, Y. P.: The Korea–United
424 States Air Quality (KORUS-AQ) field study, *Elem. Sci. Anthr.*, 9(1),
425 doi:10.1525/elementa.2020.00163, 2021.
426 Dufour, G., Hauglustaine, D., Zhang, Y., Eremenko, M., Cohen, Y., Gaudel, A., Siour, G., Lachatre, M.,
427 Bense, A., Bessagnet, B., Cuesta, J., Ziemke, J., Thouret, V. and Zheng, B.: Recent ozone trends in
428 the Chinese free troposphere: role of the local emission reductions and meteorology, *Atmos. Chem.*
429 *Phys.*, 21(20), 16001–16025, doi:10.5194/acp-21-16001-2021, 2021.
430 Gelaro, R., McCarty, W., Suárez, M. J., Todling, R., Molod, A., Takacs, L., Randles, C., Darmenov, A.,
431 Bosilovich, M. G., Reichle, R., Wargan, K., Coy, L., Cullather, R., Draper, C., Akella, S., Buchard,
432 V., Conaty, A., da Silva, A., Gu, W., Kim, G.-K., Koster, R., Lucchesi, R., Merkova, D., Nielsen, J.
433 E., Partyka, G., Pawson, S., Putman, W., Rienecker, M., Schubert, S. D., Sienkiewicz, M. and
434 Zhao, B.: The Modern-Era Retrospective Analysis for Research and Applications, Version 2
435 (MERRA-2), *J. Clim.*, Volume 30(Iss 13), 5419–5454, doi:10.1175/JCLI-D-16-0758.1, 2017.
436 Gettelman, A., Hoor, P., Pan, L. L., Randel, W. J., Hegglin, M. I. and Birner, T.: THE
437 EXTRATROPICAL UPPER TROPOSPHERE AND LOWER STRATOSPHERE, *Rev. Geophys.*,
438 49(3), doi:https://doi.org/10.1029/2011RG000355, 2011.
439 Ha, K.-J., Heo, K.-Y., Lee, S.-S., Yun, K.-S. and Jhun, J.-G.: Variability in the East Asian Monsoon: a
440 review, *Meteorol. Appl.*, 19(2), 200–215, doi:https://doi.org/10.1002/met.1320, 2012a.
441 ~~Ha, K. J., Heo, K. Y., Lee, S. S., Yun, K. S. and Jhun, J. G.: Variability in the East Asian Monsoon: a~~
442 ~~review, Meteorol. Appl., 19(2), 200–215, doi:https://doi.org/10.1002/met.1320, 2012b.~~
443 Hsu, J., Prather, M. J. and Wild, O.: Diagnosing the stratosphere-to-troposphere flux of ozone in a
444 chemistry transport model, *J. Geophys. Res. Atmos.*, 110(D19),
445 doi:https://doi.org/10.1029/2005JD006045, 2005.
446 Inness, A., Ades, M., Agustí-Panareda, A., Barré, J., Benedictow, A., Blechschmidt, A.-M.,
447 Dominguez, J. J., Engelen, R., Eskes, H., Flemming, J., Huijnen, V., Jones, L., Kipling, Z.,
448 Massart, S., Parrington, M., Peuch, V.-H., Razinger, M., Remy, S., Schulz, M. and Suttie, M.: The
449 CAMS reanalysis of atmospheric composition, *Atmos. Chem. Phys.*, 19(6), 3515–3556,
450 doi:10.5194/acp-19-3515-2019, 2019.
451 Jacob, D. J. and Winner, D. A.: Effect of climate change on air quality, *Atmos. Environ.*, 43(1), 51–63,
452 doi:https://doi.org/10.1016/j.atmosenv.2008.09.051, 2009.

453 Langford, A. O., Senff, C. J., Alvarez, R. J., Brioude, J., Cooper, O. R., Holloway, J. S., Lin, M. Y.,
454 Marchbanks, R. D., Pierce, R. B., Sandberg, S. P., Weickmann, A. M. and Williams, E. J.: An
455 overview of the 2013 Las Vegas Ozone Study (LVOS): Impact of stratospheric intrusions and long-
456 range transport on surface air quality, *Atmos. Environ.*, 109, 305–322,
457 doi:<https://doi.org/10.1016/j.atmosenv.2014.08.040>, 2015.

458 Liu, X., Bhartia, P. K., Chance, K., Spurr, R. J. D. and Kurosu, T. P.: Ozone profile retrievals from the
459 Ozone Monitoring Instrument, *Atmos. Chem. Phys.*, 10(5), 2521–2537, doi:10.5194/acp-10-2521-
460 2010, 2010.

461 Lu, X., Zhang, L. and Shen, L.: Meteorology and Climate Influences on Tropospheric Ozone: a Review
462 of Natural Sources, Chemistry, and Transport Patterns, *Curr. Pollut. Reports*, 5(4), 238–260,
463 doi:10.1007/s40726-019-00118-3, 2019.

464 McPeters, R. D., Labow, G. J. and Logan, J. A.: Ozone climatological profiles for satellite retrieval
465 algorithms, *J. Geophys. Res.*, 112(D5), D05308, doi:10.1029/2005JD006823, 2007.

466 Park, S. S., Kim, J., Cho, H. K., Lee, H., Lee, Y. and Miyagawa, K.: Sudden increase in the total ozone
467 density due to secondary ozone peaks and its effect on total ozone trends over Korea, *Atmos.*
468 *Environ.*, 47, 226–235, doi:<https://doi.org/10.1016/j.atmosenv.2011.11.011>, 2012.

469 Prather, M. J., Zhu, X., Tang, Q., Hsu, J. and Neu, J. L.: An atmospheric chemist in search of the
470 tropopause, *J. Geophys. Res. Atmos.*, 116(D4), doi:<https://doi.org/10.1029/2010JD014939>, 2011.

471 Rao, T. N., Kirkwood, S., Arvelius, J., von der Gathen, P. and Kivi, R.: Climatology of UTLS ozone and
472 the ratio of ozone and potential vorticity over northern Europe, *J. Geophys. Res. Atmos.*, 108(D22),
473 doi:<https://doi.org/10.1029/2003JD003860>, 2003.

474 Rodgers, C. D.: *Inverse Methods for Atmospheric Sounding*, WORLD SCIENTIFIC., 2000.

475 Shen, L., Jacob, D. J., Liu, X., Huang, G., Li, K., Liao, H. and Wang, T.: An evaluation of the ability of
476 the Ozone Monitoring Instrument (OMI) to observe boundary layer ozone pollution across China:
477 application to 2005–2017 ozone trends, *Atmos. Chem. Phys.*, 19(9), 6551–6560, doi:10.5194/acp-
478 19-6551-2019, 2019.

479 Shen, L., Liu, J., Zhao, T., Xu, X., Han, H., Wang, H. and Shu, Z.: Atmospheric transport drives regional
480 interactions of ozone pollution in China, *Sci. Total Environ.*, 830, 154634,
481 doi:<https://doi.org/10.1016/j.scitotenv.2022.154634>, 2022.

482 Smit, H., Straeter, W., Johnson, B. J. J., Oltmans, S. J., Davies, J., Tarasick, D. W., Hoegger, B., Stübi,
483 R., Schmidlin, F. J., Northam, T., Thompson, A. M., Witte, J. C., Boyd, I. and Posny, F.:
484 Assessment of the performance of ECC-ozone sondes under quasi-flight conditions in the
485 environmental simulation chamber: Insights from the Juelich Ozone Sonde Intercomparison
486 Experiment (JOSIE), *J. Geophys. Res.*, 112, 2007.

487 ~~Tanimoto, H., Sawa, Y., Matsueda, H., Uno, I., Ohara, T., Yamaji, K., Kurokawa, J. and Yonemura, S.:
488 Significant latitudinal gradient in the surface ozone spring maximum over East Asia, *Geophys. Res. Res.*
489 *Lett.*, 32(21), doi:<https://doi.org/10.1029/2005GL023514>, 2005.~~

490 Walker, T. W., Martin, R. V., Van Donkelaar, A., Leitch, W. R., MacDonald, A. M., Anlauf, K. G.,
491 Cohen, R. C., Bertram, T. H., Huey, L. G., Avery, M. A., Weinheimer, A. J., Flocke, F. M.,
492 Tarasick, D. W., Thompson, A. M., Streets, D. G. and Liu, X.: Trans-pacific transport of reactive
493 nitrogen and ozone to Canada during spring, *Atmos. Chem. Phys.*, 10(17), 8353–8372,
494 doi:10.5194/acp-10-8353-2010, 2010.

495 Worden, J., Jones, D. B. A., Liu, J., Parrington, M., Bowman, K., Stajner, I., Beer, R., Jiang, J., Thouret,
496 V., Kulawik, S., Li, J.-L. F., Verma, S. and Worden, H.: Observed vertical distribution of
497 tropospheric ozone during the Asian summertime monsoon, *J. Geophys. Res. Atmos.*, 114(D13),
498 doi:<https://doi.org/10.1029/2008JD010560>, 2009.

499 Yin, C. Q., Solmon, F., Deng, X. J., Zou, Y., Deng, T., Wang, N., Li, F., Mai, B. R. and Liu, L.:
500 Geographical distribution of ozone seasonality over China, *Sci. Total Environ.*, 689, 625–633,

501 doi:<https://doi.org/10.1016/j.scitotenv.2019.06.460>, 2019.
502 Yoo, J.-M., Jeong, M.-J., Kim, D., Stockwell, W. R., Yang, J.-H., Shin, H.-W., Lee, M.-I., Song, C.-K.
503 and Lee, S.-D.: Spatiotemporal variations of air pollutants (O₃, NO₂, SO₂, CO,
504 PM₁₀, and VOCs) with land-use types, *Atmos. Chem. Phys.*, 15(18), 10857–10885,
505 doi:10.5194/acp-15-10857-2015, 2015.
506 Yoon, D., Cha, D.-H., Lee, G., Park, C., Lee, M.-I. and Min, K.-H.: Impacts of Synoptic and Local
507 Factors on Heat Wave Events Over Southeastern Region of Korea in 2015, *J. Geophys. Res.*
508 *Atmos.*, 123(21), 12,12-81,96, doi:<https://doi.org/10.1029/2018JD029247>, 2018.
509 Zhang, Y. and Wang, Y.: Climate-driven ground-level ozone extreme in the fall over the Southeast
510 United States, *Proc. Natl. Acad. Sci.*, 113(36), 10025–10030, doi:10.1073/pnas.1602563113, 2016.
511
512 Schwartz, M., Froidevaux, L., Livesey, N. and Read, W. (2015), *MLS/Aura Level 2 Ozone (O₃) Mixing*
513 *Ratio V004*, Greenbelt, MD, USA, Goddard Earth Sciences Data and Information Services Center
514 (GES DISC), Accessed: [Data Access Date], 10.5067/Aura/MLS/DATA2017
515 Adler, R.F., G.J. Huffman, A. Chang, R. Ferraro, P. Xie, J. Janowiak, B. Rudolf, U. Schneider, S. Curtis,
516 D. Bolvin, A. Gruber, J. Susskind, and P. Arkin: The Version 2 Global Precipitation Climatology
517 Project (GPCP) Monthly Precipitation Analysis (1979-Present). *J. Hydrometeor.*, 4,1147-1167,
518 2003
519